Water Research 181 (2020) 115900

Contents lists available at ScienceDirect

Water Research

journal homepage: www.elsevier.com/locate/watres

Evaluating the effect of silver nanoparticles on bacteriophage lytic infection cycle-a mechanistic understanding

Eddie Gilcrease, Ryan Williams, Ramesh Goel*

Department of Civil and Environmental Engineering, University of Utah, UT, USA

ARTICLE INFO

Article history:
Received 28 November 2019
Received in revised form
10 April 2020
Accepted 29 April 2020
Available online 18 May 2020

Keywords:
Silver nanomaterial
Lytic bacteriophage
Phage capsid
Tailed phage
C-terminus

ABSTRACT

Bacteriophages and engineered nano-material (AgNPS) interactions is a relatively unexplored area of research. To answer the fundamental question whether bacteriophage lytic growth cycle is affected by the presence of AgNPs, laboratory experiments were performed with phages of *Klebsiella pneumoniae*, *Delftia tsuruhatensis, Salmonella typhimurium,* and *Shigella flexneri* using silver nanoparticles (AgNPs) with coating materials. One-step growth curves of bacteriophages indicated that the presence of these nanoparticles, and the associated ions of silver, produced pronounced effects on the lytic infection of certain bacteriophages. Effects included 96% reductions in post-infection phage yield in terms of plaque forming units (PFUs) after phages were incubated with silver nanoparticles and 28%–43% reductions from the presence of Ag^{+} alone. However, when *Klebsiella pneumonia* phage KL and *Salmonella typhimurium* phage Det7 were exposed to silver nanoparticles coated with poly-*N*-vinyl-2 pyrrolidone (PVP), an increase in final phage yield by as much as 250% was observed compared with the same phage not incubated with nanoparticles. A proposed mechanism, observed by transmission electron microscopy and verified using synthetic biology by which the nanoparticle binding phenotype can be produced, is that the binding of metal nanomaterial to phage virions results in potentially inhibitory effects. This binding was found to be dependent on the presence of exposed positively charged C-terminal amino-acid residues on the phage capsid surface, implied at first by amino-acid sequence comparisons between capsid proteins of the different phages used in this study. This was then proven experimentally using targeted DNA editing methods to fuse positive charged amino-acid residues to the coat protein C-terminus of non-binding phage. This induced the AgNP binding phenotype, as observed by TEM, DLS size measurements, and growth curve data that show the mutant constructs to be functionally inhibited after exposure to AgNPs. This research sets up a first platform for further research in the unexplored area of phage and AgNP interactions and provides useful findings.

1. Introduction

Nanotechnology has rapidly expanded with applications in electronics, contaminant remediation, toy manufacturing, drug delivery, and food processing (Oberdorster et al., 2007; Das et al., 2013; Massarsky et al., 2013). The AgNPSs most used in consumer products are silver, titanium, carbon nanotubes, iron oxide, silica, zinc, and gold with the main applications in antimicrobial protection, coatings, and health products (Juganson et al., 2015; Benn and Westerhoff, 2008). The unrestricted entry of AgNPs into the environment has been a concern for several years (Wong et al., 2017; Xing et al., 2016). In general, the toxicity of some AgNPs inactivate, or destroy, microorganisms and negatively impacts microbial and eukaryotic ecology (Sheng and Liu, 2017; Liu et al., 2017; Vazquez-Munoz et al., 2017). For example, AgNPs effectively suppress nitrifying bacteria populations, which can lead to elevated nutrient conditions in aquatic systems and reduced effectiveness of the activated sludge process in wastewater treatment (Nielsen et al., 2009; Zhang et al., 2016). Studies of material from wastewater treatment plants suggest that as little as 1.0 mg/L silver nanoparticles (AgNPs) can cause a 40% reduction in nitrification in activated sludge and dramatically reduce the growth of nitrifying bacteria *Nitrosomonas europaea*, *Nitrosococcus oceani*, and other heterotrophs (Beddow et al., 2014; Yang et al., 2014). Likewise, eukaryotic ecology has been shown to be sensitive to certain AgNPs. For example, algal growth has shown to be significantly

* Corresponding author.
E-mail address: ram.goel@utah.edu (R. Goel).

https://doi.org/10.1016/j.watres.2020.115900
0043-1354/

depressed in the presence of at least 0.9 mg/L AgNPs, and function decreases rapidly as concentration increases (Yang et al., 2014). Increased exposure to AgNPs is correlated with a decrease in chlorophyll content and reduced cell viability (Sheng and Liu, 2017).

While we have learned a great deal about the negative effects of AgNPs s on different living entities, research on the effect of AgNPs on viruses remains largely unexplored. Bacteriophages, viruses that infect bacteria, make up the majority of organisms on earth and have a profound impact on prokaryotic life everywhere, tempering microbial populations and promoting biodiversity though predation and gene transfer (Argov et al., 2017; Krystiak-Baltyn et al., 2017; Wittebole et al., 2014). The importance of bacteriophages in determining the diversity and structure of bacterial communities has been a subject of considerable research, especially in fresh water (Kenzaka et al., 2007; Brussaard et al., 2008; Matteson et al., 2011), terrestrial (Ashelford et al., 2000; Swanson et al., 2009; Wang et al., 2010), and marine ecosystems (Breitbart, 2012; Baker et al., 2014; Suttle, 2005, 2007; Weinbauer and Rassoulzadegan, 2004).

The findings (such as those presented in this manuscript) that silver nanoparticles can affect bacteriophages raises questions concerning these effects on overall microbial ecology as well as how these interactions may be exploited in a variety of applications. Despite the immense diversity of bacteriophages and their proven role in controlling microbial diversity, absolutely nothing was known prior to this study about how AgNPs interact with bacteriophages at a mechanistic level. In fact, none of the nanotoxicity and AgNPs ecotoxicity databases report about these interactions because such information is rather scarce in literature.

The overall objective of this study is to evaluate and gain understanding of nanoparticles and bacteriophage interactions with AgNPs as model nanoparticles. This is important for various reasons, including potential improvements in phage-therapy based solutions to bacteria related problems in, for example, waste-water management (Mathieu et al., 2019), and the fact that bacteriophages may act as a carrier for nanaparticles in the environment, and thus, support the transport of nanaparticles in aquatic systems. Moreover, given the degree to which bacteriophages affect aquatic bacterial ecology through their known infection cycles, understanding nanaparticles-phage interactions is imperative from an aquatic ecology point of view. The objective also included getting the first set of data in terms of their effect on phage growth cycles, and make an effort towards understanding some of the potential underlying mechanisms of the observed phage growth cycle inhibition by AgNPs. We first used *Klebsiella pneumonia* and *Delftia tsuruhatensis* as two different hosts to study interactions of their lytic phages RG2014 and KL, respectively, with AgNPs. Later, we included more hosts to expand the variety of lytic phages to study the effects of AgNP, the associated ions of silver, and the presence of PVP (a coating used for stabilization of some nanoparticles) as they relate to phage infectivity. Finally, we used synthetic biology (specifically, the targeted DNA editing of a phage model system) to modify surface characteristics of the phage capsids to get a deeper understanding about phage-AgNPs interactions. The results obtained lay down a foundation for further research and provide the very first report, along with a mechanistic understanding, of phage-AgNPs interactions.

2. Materials and methods

2.1. Host bacteria studied

To begin the study, two primary lytic phages and their hosts were used in these experiments. One of the host bacteria used, *Klebsiella pneumoniae* ATCC BAA-2146 (Yong, 2009) is a Gram-negative, non-motile, encapsulated, rod-shaped bacteria. First isolated from a US hospital patient in 2010, it carries the antibiotic resistance gene New Delhi metallo-β-lactamase 1 (NDM-1), which confers resistance to a broad range of beta-lactam antibiotics, a mainstay for the treatment of bacterial infections (Yong, 2009). This strain was obtained from the American Type Culture Collection (ATCC) facility in Manassas, Virginia. The second host selected, *Delftia tsuruhatensis* ARB-1, is a Gram-negative, rod-shaped, motile bacteria originally isolated from a wastewater treatment plant in Utah in Dr. Ramesh Goel's lab using methods described by Bhattacharjee et al., 2015. In addition to these two hosts, *Shigella flexneri* (Casjens et al., 2004) and *Salmonella enterica* serovar *typhimurium* LT2 (McClelland et al., 2001) were also used as hosts to reflect a variety of phage morphologies and host strains.

2.2. Lytic phage isolation, characterization and purification

Both host bacteria were grown in Luria Broth (LB) (Miller, 1972) media for growth at 37 ± 2 °C. Mixed liquor biomass was obtained from a local wastewater treatment plant and used as a source of phages to isolate lytic phages for bacterial hosts *K. pneumoniae* and *D. tsuruhatensis*. The lytic phages KL, infecting *K. pneumoniae,* and phage RG2014 infecting *D. tsuruhatensis* were isolated following protocols previously described (Bhattacharjee et al., 2017; Hockett and Baltrus, 2017). A phage titer of the lysate stock and a TEM analysis of the lytic phage was performed as described in our earlier study (Kotay et al., 2011).

All phages were purified from individual plaques and propagated by infection of their respective hosts in liquid culture (Earnshaw et al., 1976). Phages were purified by cesium chloride density gradient centrifugation (Tang et al., 2006) in an SW41 Ultraclear centrifuge tube (for SW41 Beckman rotors). Concentrated phage lysate was layered atop a step gradient consisting of 10% Sucrose + SMG, 1.4 g/mL CsCl + SMG, and 1.6 g/mL + SMG separated by phase, in that order, from top to bottom. These preparations were then centrifuged at 220,000*g* for 2 h at 20 °C. The band containing phage, located at the 1.4/1.6 CsCl interface, was extracted with a syringe and dialyzed against SMG buffer using a Spectra/Por™ 7 50,000 MWCO dialysis membrane. Measurement of the protein concentrations of purified phage was done using the Qubit™ Protein Assay Kit (Cat# Q33211).

2.3. Other reference lytic phages studied

After testing the lytic phage for two host strains (e.g., *Klebsiella pneumoniae* ATCC BAA-2146 and *Delftia tsuruhatensis* ARB-1), we also used the *podoviridae* phage SF6 of *Shigella flexneri* (Casjens et al., 2004) as well as a variety of other well-studied phages belonging to different families infecting *Salmonella enterica* serovar *typhimurium* LT2 (McClelland et al., 2001); P22 (*podoviridae*), SP6 (*podoviridae*), 9NA (*siphoviridae*), and Det7 (*myoviridae*)) (Pedulla et al., 2003; Dobbins et al., 2004; Casjens et al., 2014; Casjens et al., 2015) so as to reflect a variety of phage morphologies and host strains in our testing with AgNPs. The P22 strain used (UC-937) is a temperate phage that has been heavily modified for use in the DNA editing methods described later. It carries a knockout of gene c1 which represses transcription of lytic genes obligating it to the lytic life cycle (Tokuno and Gough, 1975), the chloramphenicol resistance gene (CamR), and an amber mutation in the "holin" gene (gp13-) that inactivates lysis unless grown in a host suppressor strain (S. typhimurium + supE). SF6, P22, SP6, and 9NA were purified using the same protocol detailed earlier and dialyzed in 1X SMG buffer, the preferred buffer of RG2014, and for which the other phage tested appeared stable based on plaque assays over time

(data not shown). The final concentration of SMG, when in use, was .5X SMG after 1:1 dilution with nanoparticle solutions. Phages were also dialyzed in 2X TM buffer to assess any observable difference phage/nanoparticle interactions when using a lower ionic strength buffer (1X TM after dilution with nanoparticle solution). All experiments using P22 fusion mutants were conducted using phage dialyzed in 2X TM buffer (the standard buffer of P22 is 1X TM, and the final concentration used in experiments after dilution). Det7 proved to be unstable in cesium chloride gradients, and so was purified by repeated centrifugation (6000*g*), filtration through a 0.45 nm filter, and centrifuged through 10% sucrose (SW41 rotor, 220,000*g*) followed by resuspension in 2X TM or SMG buffer.

2.4. Nanoparticle types and characterization

In this manuscript, "bare" AgNPs refer to uncoated AgNPs in sodium citrate, and "coated" refer to AgNP coated with poly-*N*-vinyl-2 pyrrolidone (PVP) for stability. The "NanoXact" silver (AgNP) spherical nanoparticles were obtained from NanoComposix in sizes of 10 nm, both uncoated ("bare", stored in 2 mM sodium citrate) and PVP coated (stored in H_20). "Biopure" versions of these nanoparticles, available at higher concentrations (1 g/L) and quality, were also purchased. Other stock specification details of the nanoparticles used are provided in Table 1.

Zeta-potential (ζ) values for nanoparticles were obtained via dynamic light scattering (DLS) (Malvern Panalytical Zetasizer Nano ZS) and are given as the average of [n = 3] scans. (Table 1). Nanoparticles were diluted to concentrations of 2.0 mg/L in various dispersion media; TM (10 mM Tris-HCl, 1 mM $MgCl_2$ pH = 7.5), SMG (50 mM Tris-HCl pH = 7.5, 100 mM NaCl, 10 mM $MgSO_4$, 0.01% gelatin), 2 mM sodium citrate, or H_2O. Transmission electron microscopy conducted on the AgNP stock solution confirmed uniform size distribution and very little or no agglomeration of AgNPs in solution.

2.5. Bacteria and AgNP interactions

AgNPs have been shown to be lethal to prokaryotes. As a control to assess the impacts of AgNPs during culture, we tested host strains *Delftia tsuruhatensis* and *Klebsiella pneumoniae* for their response to AgNPs used in this study. 25 mL of each strain was grown to mid-log phase in a 250 mL flask at 37 ± 2 °C in an orbital shaker (190 RMP). 1 mL from each culture was then incubated at room temperature for 5 min with different concentrations of bare-silver nanoparticles; 0.025 mg/L, 0.25 mg/L, and 1.25 mg/L. Controls, in which cultures were not incubated with nanoparticles, were prepared for each strain. The cultures were then centrifuged at 3000 *g* at room temperature for 3 min, decanted, and resuspended with 1 mL LB. These resuspensions were then added to 25 mL LB in 250 mL flasks and shaken at 37 ± 2 °C for 70 min. This is the same incubation time used post infection in most infectivity experiments and is sufficient for comparative measurements of growth. 1 mL from the cultures was then placed on ice for 10 min, serially diluted in LB and plated onto LB Agar plates. Plates were incubated overnight at 37 ± 2 °C, after which colonies were counted visually [n = 1]. To assess the impact of citrate present in bare AgNP stocks, phages were incubated in 1 mM Na-citrate in parallel with, and in the same manner as, the described growth curve experiments as a control [n = 1].

2.6. Nanoparticle and phage interactions

Our primary method of study for phage-nanoparticle interactions was the measurement of the effect of nanoparticles on phage one-step growth curves and total phage yield after 70 min of infection. A one-step growth curve defines the rate at which, during bacteriophage infection of its host, the phage is attached to the bacterium, injects its genetic material, and produces more phage progeny, which burst from the cell upon completion of the lytic cycle. For one-step growth curve experiments, purified phage, stored in SMG or 2X TM buffer, was added to 10 mg/L concentrations of nanoparticle solution at a 1:1 vol ratio, with a final phage concentration of 5×10^8 PFU/mL and final buffer concentration of 0.5X SMG or 1X TM. This solution was incubated for 30 min at room temperature in 2 mL polypropylene microcentrifuge tubes. A volume necessary to achieve a multiplicity of infection (MOI) of 0.0625 phage per host bacterium was then transferred to 1 mL of host cells at mid-log phase in LB and incubated at room temperature for 5 min. Cells were then pelleted by centrifugation for 3 min at 3000*g*, decanted, and resuspended in fresh LB. This resuspension was transferred to a 25 mL host culture at mid-log phase in a 250 mL flask and shaken (190 RPM) at 37 ± 2 °C for 70 min.

For detailed analysis of bacteriophage growth curve effects for RG2014 and *K. pneumonia phage KL* only, 1 mL culture quantities were collected every 10 min as the infection proceeded. These cultures were then immediately treated with chloroform, vortexed,

Table 1
Properties of nanoparticles and phage used in the study.

Nanoparticles	Stock Buffer	Conc	pH	Particles/mL	ζ stock	ζ TM
10 nm AgNP (Bare)	2 mM Citrate	0.02 mg/mL	7.7	3.7E+12	−31 mV	−27.9 mV (n = 3)
10 nm AgNP (PVP)	H_2O	0.02 mg/mL	6.4	3.5E+12	−26 mV	−19.1 mV (n = 3)
Phages	**ζ Virions**	**C-Term AA Sequence**			**Q C-term**	**%PFU/[n = x]**
RG2014 [49]	−14.8 mV	YGILFL**R**PE**R**IGII**K**TVAP**R**			+1.61	8.84 ± 17.5/[n = 5]
KL	−12.4 mV	KGGLP**K**LDGTEIIDPQA**KFRR**			+1.61	40.5 ± 8.5/[n = 5]
Det7 [54]	−15.5 mV	DGIAQDSNVYF**RK**GLI**K**SLF			+2.61	41.4 ± 3.2/[n = 3]
P22 [51]	−17.5 mV	YGVNAT**R**PEAIGVGLPGQTA			−0.39	72.6 ± 16.3/[n = 3]
P22 gp5:F1	−18.1 mV	GVGLPGQTATAPGAGAGAN			−0.39	82.5 ± 3.5/[n = 3]
P22 gp5:F2	−13.4 mV	IGVGLPGQTASGSGS**KA**R			+1.61	9 ± 1/[n = 5]
P22 gp5:F3	−13.3 mV	GAIGVGLPGQTASGSG**SRR**			+1.61	27.5 ± 2.5/[n = 3]
SP6 [52]	−18.3 mV	AV**R**AVMANDI**K**PTAL**K**PTEE			−0.39	105 ± 9.1/[n = 3]
9NA [53]	−17 mV	FAIDVQMVAPDLGILFYDAV			−2.39	72 ± 20.7/[n = 3]
SF6[50]	−15.3 mV	LLPAYVCFNPHMGGQFFGNP			−0.27	108 ± 8.3/[n = 3]

Zeta-potential (ζ) stock measurements were obtained from nanoparticles diluted in the same buffers, and at the same pH values, in which they were received (in H_2O or 2 mM sodium citrate). (ζ) TM values for nanoparticles and phage were obtained after dilution in TM, pH = 7.5 [n = 3]. The last 20 amino acids of the capsid protein C-terminus are noted. Positive charged amino acids are in bold and negative charged amino acids are underlined. The P22 sequence of the fusion mutants (gp5:F*n*) are highlighted. Q C-term denotes the charge of the last 10 amino acids. Q = coulombs divided by the elementary-charge constant. %PFU is the percentage of plaque forming units (with standard deviation and repeat numbers, n) present after 70 min infection with phages that had been incubated with 10 mg/L 10 nm Bare AgNPs compared with a "no nanoparticles" control (data from Figs. 3b and 4).

and centrifuged at 6000*g* for 5 min, after which the supernatant was collected and plaque forming units (PFU) were measured. In all other cases, the data was collected only at 70 min as the yield at the end of this time consistently reflects the efficiencies of the viral infections being compared. This was based on the detailed growth curve data from KL and RG2014 (and t = 70-minute titrations of the other phage used in this study) that suggested growth to be sufficiently substantial at this time point for comparative analysis. All phages used in this study were directly titered on their respective hosts after incubation with AgNPs, in which 1×10^{10} PFU/mL phage were incubated in 10 mg/L 10 nm bare AgNPs for 30 min at room temperature.

To determine whether background Ag^+ present in the stock nanoparticle solution has an effect independent of the presence of nanoparticles, stock nanoparticle solutions were diluted 2X separately in H_2O or SMG and centrifuged at 194,000*g* for 90 min using a SW55Ti Beckman rotor. This is done to remove nanoparticles and other insoluble products from nanoparticle solutions, thereby isolating Ag^+. The Ag^+ present in these supernatants was quantified by ICP-MS using an Agilent 7500ce, quadrupole mass-spectrometer. These solutions were then used to infect cultures by the one step growth curve method described. The volume of nanoparticle solution containing no AgNPs used in these experiments was identical to that used in the 10 mg/L nanoparticles growth curve experiments.

To isolate effects seen from PVP when used as a coating for AgNPs, experiments were conducted using PVP powder (average mw = 40,000 amu) dissolved in sterile milliQ pure water to 20 mg/L stock solution. One-step growth curve measurements [n = 2] for phage incubated with 2X diluted PVP solution with a final concentration of 10 mg/L were conducted in the same manner as detailed earlier. DLS size data for phage/AgNP interactions was obtained by incubating 1×10^{11} phage with 10 mg/L AgNPs for 30 min. This was then diluted 10x into TM buffer and applied to the Malvern Zetasizer with values given as the average of [n = 3] scans.

2.7. Construction of positively charged C-terminal P22 coat protein extensions

Salmonella P22 prophage strain UC-937 was used to genetically fuse peptide extensions of positively charged amino-acid residues (arginine and/or lysine) to the C-terminus of coat protein (P22 gp5) by a serine-glycine linker (SGSGS). The peptide fusions constructed have properties detailed in Table 1. One of the three peptide sequences chosen, Gp5:F1, resulted in a non-functional phage product once constructed, likely due to improper folding of the coat protein. This peptide sequence lacks the SGSGS linker but remained relevant to the study. DNA editing was done using the Lambda-Red Mediated Galk (galactokinase) Recombineering methods described in (Marinelli et al., 2012). The Salmonella strain carrying the P22 prophage UC-937 and the plasmid pKD46 (expressing the recombinase Lambda-Red) was grown in LB + 50 μg/mL ampicillin and 0.2% arabinose to OD_{595} = 0.7. Cells were then harvested and made competent for electroporation (O'Callaghan and Charbit, 1990). Using PCR (GoTaq™ Mastermix Cat#M7133 and the recommended cycling conditions from product literature), the gene Galk was amplified from the plasmid pGalk using primers that added 50 base-pair (bp) 5′ and 3′ tails containing DNA sequence homology to regions flanking the site to be edited, that is, the 3′ end of P22 coat protein (gp5). This product was used for linear DNA transformation (electroporation) of the above cells. The Galk+ phenotype was then selected for on minimal media containing 0.4% galactose. Replacement DNA, containing the final modified sequence, was constructed by PCR amplification of wild type P22 DNA using primers that supply sufficient tails of homology to regions flanking the Galk site of the above transformant. This product was used for transformation of the Galk+ knock-out strain in the presence of Lambda-Red. Galk- cells (cells presumed to be successfully edited) were selected for using minimal media containing 30 μg/mL chloramphenicol (for retention of the prophage) and deoxy-galactose which produces a toxic compound after being metabolized. Colony candidates were struck out onto LB + chloramphenicol. The correct insertion of the sequences was confirmed by PCR amplification of colonies, followed by Sanger sequencing of PCR products. Primer sequences for amplification of Galk insertion and replacement DNA, using wild type P22 as the template are in Table S1.

2.8. Transmission electron microscopy

For TEM visualization of nanoparticle/phage interactions, 2×10^{11} PFU/mL phage dialyzed in 2X TM or 1X SMG were mixed with an equal volume of 20 mg/L nanoparticles in their respective stock buffer (either 2 mm sodium citrate, or H_2O). After 30 min at room temperature, 3 μl of this mixture was laid onto Formvar 400 Mesh Copper grids. After 1 min, the excess phage solution was removed with filter paper. 3 mL of 1% uranyl acetate was then added to the grid, left for 1 min, and then removed with filter paper. All negatively stained TEM images were obtained using a TEM model JEOL JEM-1400.

2.9. Statistical analysis

%PFU values were determined by dividing the PFU of the nanoparticle exposure test subject by the control (no nanoparticle exposure). This was done for each repeat number. The %PFU given is the mean of these experimental repeats with p-values obtained from an unpaired *t*-test. Significance was determined at an alpha level of 0.05 ($p \leq 0.05$).

3. Results and discussion

3.1. AgNPs and phage zeta-potential characteristics

Upon taking DLS zeta-potential measurements of nanoparticles diluted in SMG, the primary physiological buffer used in these experiments, we observed significant precipitation and increases in millivolt values (from high negative to low negative). High salt concentrations are known to cause an increase in current, heat, and ultimately a thinning and collapse of the electrical double layer, resulting in significant reduction of zeta-potential (Dukhovich et al., 2003; Skoglund et al., 2017). When particles were diluted in a lower ionic strength buffer such as TM (10 mM Tris pH = 7.5, 1 mM $MgCl_2$), the values upon measurement aligned more closely with those of the stock medium. Since the effects of nanoparticle interaction are observable in either TM or SMG, these are the values used for comparative analysis. All nanoparticle types produced negative values, with PVP coated nanoparticles having consistently lower negativity when compared to uncoated silver nanoparticles in H_2O (Table 1). The PVP coatings on some AgNPs are largely present to reduce aggregation in higher salt concentrations (which may hinder biological activity), and to reduce toxicity in higher organisms (Mirzaei et al., 2017). The tradeoff is shorter shelf life in stock solution due to a greater instability (compared with bare particles) in H_2O, and a lower reaction potential (negativity) as noted in zeta-potential specifications (Mirzaei et al., 2017).

DLS size analysis of nanoparticles diluted in SMG suggested the presence of aggregation and production of precipitate, while the phage and nanoparticles diluted in TM did not yield errors related to precipitation and yielded values in line with those expected. Nearly all of the components of SMG (50 mM Tris-HCl pH 7.5,

100 mM NaCl, 10 mM $MgSO_4$, and 0.01% gelatin) (Kapoor et al., 1994), are capable of reacting with silver ions which are being slowly shed from the nanoparticles over time. Much of this precipitate likely consists of destabilized nanoparticles and insoluble compounds of Ag^+ with buffer components, as detailed later in section 3.7. Experimental data, also discussed later, does not suggest co-precipitation of phage and nanoparticles as a mechanistic explanation for the effects observed. The effects described in this report are seen experimentally when phages are incubated with nanoparticles in SMG or TM buffers, so it can be presumed that the sedimentation or agglomeration observed though DLS when SMG is used does not prevent phage interaction with nanoparticles or influence the observed effects on infection.

For phage-AgNPs interaction experiments, the magnitude of the surface charge of particles was inferred by measurement of the zeta-potential. The zeta-potential is a measure of the electric field potential difference between the dispersion media (in this case TM, SMG buffer, 2 mM sodium citrate, or H_2O) and the layer of fluid attached to the particle (nanoparticles or phage). While not equal to the surface potential of a particle, zeta-potential can be used to approximate the magnitude of the surface charge (Bhattacharjee, 2016). Table 1 shows the zeta potentials of the two isolated phages (*Delftia tsuruhatensis* phage RG2014, and *Klebsiella pneumoniae* phage KL) as well as the five other phages obtained from a different laboratory, and the four P22 mutant constructs. Table 1 also shows the C-terminal coat protein (capsid) sequence of each phage. All phage species diluted in TM produced zeta-potential values that were negative and similar to one another.

3.2. Bactericidal effects of AgNPs on host strains

Several publications have shown bactericidal effects of AgNPs on model bacterial populations (Seil. and Webster, 2012; Dakal et al., 2016). In an attempt to evaluate this possibility with the host strains used, cells were treated with concentrations of bare and PVP coated nanoparticles identical to those used in the one-step growth curve experiments of phages, and subjected to the same incubation and wash protocol. After 70 min of growth (the average time used for phage growth curve experiments), no significant difference in colony forming units (CFU) (Fig. S1), or spectrophotometric absorbance was observed in cells treated with nanoparticles as compared to cells not treated with nanoparticles. While bactericidal effects have been observed at these concentrations in other systems (Seil. and Webster, 2012), the short periods of exposure used in this study prior to dilution appear to have little if any effect on growth of the strains examined under our conditions. Nevertheless, these results confirmed that AgNPs were not inhibitory to both bacteria at tested concentrations of AgNPs.

3.3. The first experimental evidence of the effect of AgNPs on phage growth cycle

First, we tested the effect of silver AgNPs on the growth cycles of lytic phages KL of *K. pneumonia* and RG2014 of *D. tsuruhatensis*. These lytic phages represent two distinctly different families of lytic phages, with RG2014 belonging to *podoviridae* (the short-tailed phages) and KL to *siphoviridae* (long-tailed phages). In these experiments, we used higher concentrations of AgNPs (particularly during the phage/nanoparticle incubation step) than are generally present in the environment. This was done for different reasons; (1) there are no reports concerning concentration range as it relates to dose/response available for AgNP/bacteriophage interactions, and (2) we wanted to evaluate these interactions under worst case scenarios such as those where researchers initially used much higher concentrations of AgNPs to evaluate their effect on prokaryotic ecology under lab scale conditions (Sheng and Liu, 2017; Liu et al., 2017; Vazquez-Munoz et al., 2017). Nevertheless, these experiments promise to establish baseline information about AgNP-phage interactions which could be useful for future design of new experiments.

It should also be noted that LB, the growth media used for all infectivity experiments, contains peptides and proteins that chelate, or otherwise react, with silver ions (Corbisier et al., 1999). Since the effects described were observable and statistically significant using LB, it was deemed reasonable to examine the effect of silver nanoparticles and their ions using semi-physiological conditions, in the sense that LB is optimized for growth of these bacteria, as opposed to non-chelating buffers typically used in the study of ion-based toxicity.

Uncoated AgNPs come in 2 mM sodium citrate as a suspension buffer. It is known that some concentrations of sodium citrate negatively affect phage infectivity (Shafiai and Thompson, 1964). To determine whether sodium citrate at the concentrations used has an effect on phage infectivity during experiments, a one-step growth curve was conducted using phage in 1 mM sodium citrate without prior incubation with nanoparticles. No effect from the citrate was observed under the conditions used (Fig. S2).

Fig. 1a and b shows one-step growth curves in LB for phage RG2014 (infecting *D. tsuruhatensis* ARB-1) and phage KL (infecting *K. pneumoniae*) with 10-min intervals of data after the phage were incubated with 10 mg/L of uncoated and PVP-coated silver nanoparticles in 0.5x SMG. As stated in the Methods section, SMG buffer contains components known to react with silver nanoparticles and their associated ions. Gelatin, in particular, is known to chelate silver ions in solution, thus reducing bioavailability. In these experiments, the final concentration of gelatin after dilution (0.005%) is very low relative to studies that describe such interactions (Kapoor et al., 1994). Adverse effects on phage lytic growth cycle after AgNP incubation were seen during infections of both phages. In these experiments, uncoated bare silver nanoparticles reduced infection yields of phage RG2014 by 89% [n = 1] and phage KL by 92.4% [n = 1] after 70 min of infection as compared with control experiments (black circles, where the phage mixture was not incubated with AgNP) that showed normal phage infection of its host bacteria. PVP-coated silver nanoparticles reduced the post infection PFU of RG2014 by 74% [n = 1] (black squares). To our surprise, PVP-coated silver AgNPs increased the yield of phage KL by 192% [n = 1] as shown by inverted black triangles in Fig. 1b. Growth curve experiments were also conducted lasting beyond 70-min for phage KL, which demonstrated total lysis of culture to occur after 80 to 90-min (See Fig. S3). Much like in Fig. 1b, Fig. S3 also shows significant differences in PFUs for KL phage when incubated with AgNPs as compared with the control. As sufficient growth and effects from AgNPs were consistently observable at t = 70 minutes for phage KL as well as the additional phages used in this study, this is the time point set for measurement of infectivity in all downstream experiments.

The observed increase in yield of phage KL, but not of RG2014, with PVP coated silver nanoparticles prompted us to perform more control experiments using pure PVP powder (presented later in this paper). Phage KL was incubated with 10 mg/L bare silver AgNPs, 10 mg/L PVP-coated silver AgNPs, and pure PVP power dissolved to 10 mg/L. Phage incubated with dissolved PVP powder was observed to have a similar elevation in phage yield as phage incubated with PVP-coated silver nanoparticles [n = 2]. **(**Fig. 1c**).** This suggests that the presence of PVP alone is sufficient to produce this effect in phage KL and has nothing to do with the presence of AgNPs in the case of phage KL. The shedding of silver ions from PVP-coated silver nanoparticles destabilizes them, potentially causing the PVP, held to the particle by weak van der Waals forces, to be released into solution at an unknown rate. This de-stabilization occurs over time

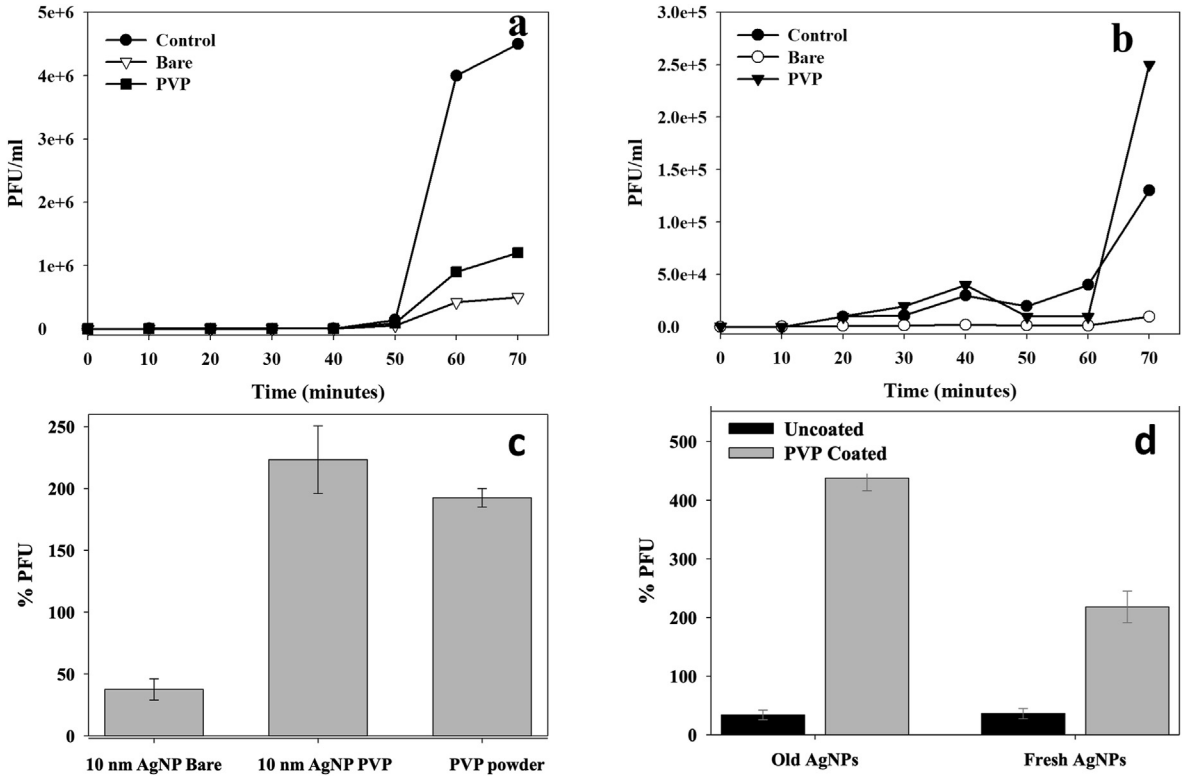

Fig. 1. One step growth curves of **(a)** [n = 1] phage RG2014 and **(b)** [n = 1] phage KL after incubation with bare and PVP-coated AgNPs in .5 SMG. **(c)** [n = 2] Post growth curve % PFU of phage KL after incubation with AgNPs and dissolved PVP powder as compared with controls not incubated. **(d)** [n = 2] Post growth curve % PFU of KL after incubation with 6 weeks "Old" AgNPs vs. freshly received "New" AgNPs compared with non-incubated controls. Error bars indicate standard deviation.

in nanoparticle stock solution, and is increased in salt containing buffer solutions (Levard et al., 2013). This may result in the production of "free" PVP in solution which, in the case of silver AgNPs, is more likely to react with the virions to produce the observed effects than when bound as nanoparticle coating. It was observed, in fact, that PFU yields of phage KL were significantly higher when incubated with PVP-Silver that was over a month old (from the date of purchase) compared to recently purchased nanoparticles used immediately after the receipt from the manufacturer [n = 2] (Fig. 1d).

To verify the findings that PVP coated silver AgNPs caused an increase in yield in phage KL, we conducted further experiments that included phage Det7, a *myoviridae* phage infecting *Salmonella enterica* serovar *typhimurium* LT2, and several other phages belonging to different phage families. All the phages used in this study were exposed to PVP-coated nanoparticles (results further discussed in Section 3.5 and Fig. 3b), and only KL and Det7 phages were shown to display an increase in phage function. KL and Det7 phages have very different tail morphologies *(siphoviridae* and *myoviridae* respectively), and the only other *siphoviridae* tested (9NA) does not have a positive response to PVP. Structural comparisons between phage, therefore, provide few clues as to mechanism. Low concentrations of PVP has been reported to stabilize some proteins, acting as a crowding agent that reduces aggregation under some conditions (Gombotz et al., 1994; Huan-Xiang, 2013). TEM images of KL particles do not appear to be aggregated, however specific viral or host proteins involved in the attachment mechanism of these phages may be affected by PVP in such ways. While interesting, these mechanisms are subject to a different set of experiments outside the scope of this paper.

3.4. Transmission electron microscopy for phage-AgNP interactions

TEM was conducted on phage mixtures incubated with AgNPs to determine any resulting structural changes. Phages RG2014 and KL were incubated with AgNPs at various concentrations for 30 min at room temperature, after which it was observed by TEM that the majority of nanoparticles tended to be bound to the virions without evidence of aggregation. (Fig. 2a–c).

To determine whether nanoparticles would remain attached to phage post cesium chloride purification, phage mixtures were incubated in a different set of experiments with 10 mg/L and 500 mg/L "Biopure" 10 nm AgNPs nanoparticles, both bare and PVP coated, for 30 min at room temperature. Thereafter, incubated phages were purified by cesium chloride step gradient centrifugation. The purified phage samples were examined by TEM and were determined not to have any nanoparticles attached to them, nor to have any noticeable structural changes. Hypothetically, if strong interactions between AgNPs and phages occurred, "heavier" phages are not expected to be in the same density layer the free phages. In that case, either two layers will be seen in cesium chloride purification and/or heavy loss of phage numbers will be recorded post ultracentrifugation. However, we did not see either two bands or loss of phages post ultracentrifugation. Next, the cesium chloride purified phages, which were initially incubated with nanoparticles, were diluted to the same protein concentrations as a control (cesium purified, but not incubated with nanoparticles) and used to infect the host using the described one-step growth method. After 70 min of infection, no significant effects on PFUs levels were observed (Fig. 3a). This is in contrast with experiments conducted simultaneously using phage that were not cesium purified after

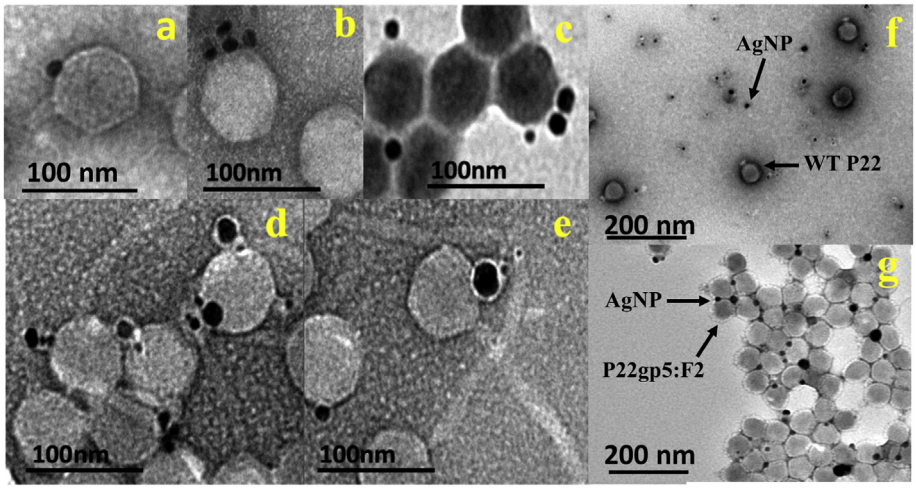

Fig. 2. (a, b) *Delftia* Phage RG2014 with bare AgNPs in 0.5X SMG. (c) RG2014 with PVP AgNPs in 0.5X SMG. (d, e) *Klebsiella* Phage KL with PVP AgNPs in 0.5X SMG. (f) Wild-type P22 with bare AgNPs in 1X TM. (g) P22gp5:F2 mutant with bare AgNPs in 1X TM.

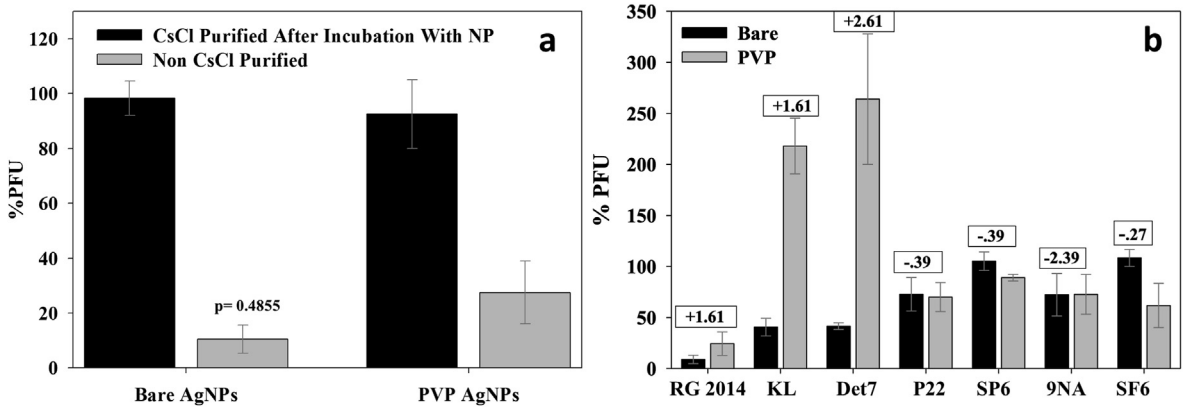

Fig. 3. (a) [n = 3] Post growth curve %PFUs of phage RG2014 (compared with no-nanoparticle controls) that had been incubated with AgNPs in .5X SMG followed by cesium chloride step-gradient purification vs. not purified. (b) [n ≥ 3] Post growth curve %PFUs of a variety of phage tested with bare and PVP-coated AgNPs in .5X SMG. Boxed values represent the charge number of the last 10 amino acids of the coat protein at pH = 7.5 (Q of C-terminus). Error bars indicate standard deviation.

incubation with nanoparticles and which did show significant reductions in PFUs (Fig. 3a). Mechanistically, these data suggest that the bonding of AgNPs with phages is not strong enough to allow AgNPs to remain attached to phages during cesium chloride purification, and that no permanent structural changes are incurred (at least under these tested conditions) that produce inhibitory effects on infection after nanoparticles are removed.

3.5. Further confirmation of inhibitory effects of AgNPs on phage growth cycle using additional phage types and a mechanistic understanding

To further test the effects of nanoparticles on infection of liquid bacterial cultures, five additional phages were selected to include representatives from the families *myoviridae* (Det7), *siphoviridae*, (9NA), and *podoviridae* (P22, SP6, SF6). These along with the other two phages used in this study were incubated with AgNPs in 0.5X SMG and used to infect their host. After 70 min of growth, the PFU in the cleared lysates were measured with the results shown in Fig. 3b. As evident from Fig. 3b, different phages are shown to be affected in different ways by different types of nanoparticles. *Delftia* phage RG2014, when incubated with bare AgNPs, produced up to 92% ± 4 [n = 5] ($p < 0.05$) fewer plaques, closely aligning with what was reported earlier in this manuscript, after 70 min of shaking compared to the plaques produced in the control. Phage KL produced 60% ± 7.5 [n = 5] ($p < 0.05$) fewer plaques after exposure to bare silver nanoparticles. After KL exposure to PVP silver nanoparticles, PFU yield increased to 218% ± 21 [n = 5] ($p < 0.05$) compared with the control. Phage Det7 showed similar results as KL, to include an even larger increase in PFU after incubation with PVP silver nanoparticles: 263% ± 63.9 [n = 3] (p=<0.05) Phages P22 [n = 3] ($p < 0.05$) and 9NA [n = 3] ($p = 0.08$) showed roughly 28% ± 16 reductions in PFU when exposed to bare and PVP-coated silver nanoparticles. Phage SP6 [n = 3] ($p > 0.05$) and SF6 [n = 3] ($p > 0.05$) showed no statistical reduction in PFU after exposure to silver nanoparticles.

TEM images clearly depict nanoparticles sticking to the capsids of RG2014 and KL phage particles (Fig. 2) and not to P22 (Fig. 2f). This suggests that the binding of nanoparticles to phage is related to the observed inhibitory effects on infection. It also suggests that the exposed regions of the viral coat proteins of RG2014, KL, and Det7 share nanoparticle binding features strong enough to overcome the weaker repelling forces between the negatively charged surfaces of phage and nanoparticles that P22, 9NA, SP6 and SF6 lack. One such feature may be the presence of positive charges near the C-terminus of the major capsid protein, a region likely to extend

from the surface of the capsid (Servid et al., 2013) and a hypothesis we propose to test. For further demonstration of the observed phage-AgNP interactions, Table 1 lists properties of the different phages tested to include zeta-potential measurements, the C-terminal peptide sequence of the capsid protein, the charge number (Q) of the last 10 residues, and the PFU percentage of surviving phage after exposure to bare silver nanoparticles. As evident from this table, phages RG2014, KL and Det7 have positive charges in this region, and were also shown to be negatively affected by silver nanoparticles. In contrast, other phages with negative charges at this location were either affected to a smaller degree or not at all by AgNPs. These preliminary results imply a relationship between inhibition of phage lytic cycle and phage coat protein C-terminus composition with the magnitude of these local charges appearing to correlate with both the ability to bind nanoparticles and the inhibitory effect of nanoparticles on infectivity (Table 1, Fig. 3b).

3.6. Effect of AgNPs on phage mutants with positively charged C-terminal P22 coat protein extensions

Double stranded DNA (dsDNA) tailed phages major capsid proteins generally share a common protein fold, but often have little recognizable amino-acid sequence similarity. There is usually an outer negatively charged region exposed to the surface, and an inner positively charged region that allows the phage capsid to interact with the negatively charged DNA to form a stable container (Tresset et al., 2017). In cases where the 3D structures of these proteins are experimentally known, the C-terminus is often exposed at the surface and at varying distances (Fig. S4) (Servid et al., 2013; Duda et al., 1995; Kizziah et al., 2017). Positively charged amino-acid residues at this position would grant a distribution of positive charge over the surface, via multiple 5- or 6-unit rings, scattered around the capsid that could enable the observed binding effects even while the global interaction potentials of both interacting bodies are negative and repulsive in nature.

To test the hypothesis that exposed, positive coat protein C-termini of phages are associated with nanoparticle binding and greater susceptibility to silver AgNP inhibition, an attempt was made to induce the nanoparticle binding phenotype by using synthetic biology to attach positively charged amino-acid residues to the C-terminal end of coat protein. Bacteriophage P22 was chosen as the model system since it is not observed to bind to nanoparticles, and has a well characterized capsid structure appearing to possess no surface positive charges (Hryc et al., 2017). Lambda-red mediated Galk recombineering methods were used to construct three separate P22 coat protein (gp5) C-terminal fusions (Table S1). P22gp5:F1 (P22-VGLPGQTA:**PGAGAGAN**) is a control mutant with an 8 amino-acid extension having a small negative charge similar to wild type P22 at the C-terminus (Q = −0.39). P22gp5:F2 (P22-VGLPGQTA:**SGSGS-KAR)** consist of an 8 amino-acid extension that includes a serine-glycine linker followed by a positively charged amino-acid sequence, and P22gp5:F3 (P22-VGLPGQTA:**SGSGS-RR**) is similar to F2 except that the SG linker is followed by two positive arginine residues.

These mutants, after purification, were incubated with bare silver nanoparticles for 30 min at room temperature in 1x TM Buffer, the standard buffer of P22. TEM images show the two mutants with positive C-terminal coat protein charges to have acquired the nanoparticle binding phenotype as compared to the wild-type P22 control and the negatively charged control construct (Fig. 2f). Size scattering measurements were taken using DLS equipment for wild type and mutant P22 phages after incubating them with silver AgNPs. Fig. S5 shows the scatters for the different conditions tested. The average size of wild-type phage in solution show no noticeable shift when incubated with AgNP; 72.01 nm−80.04 nm (panels a and b in Fig. S5). On the other hand, the P22 coat protein (gp5) mutant with positive charge at C-terminus (P22gp5:F2) shows significant shift in average size, from 97.84 nm−156.3 nm (panels c and d in Fig. S5).

In growth curve experiments [n = 3] ($p < 0.05$), the mutant phages with positive C-terminal charges show substantial inhibition of infection from exposure to silver nanoparticles that the wild-type strain, and mutant control, lack (Fig. 4a). This suggests that the nanoparticle binding feature, and the resulting inhibition of infection, is indeed related to these exposed positively charged residues on the capsid, and that these features can be artificially produced by genomic editing methods.

It is likely that the mechanism by which the metal nanoparticles disrupt phage functionality derive, in part, from the binding of nanoparticles across the surface of the phage capsid. TEM images do not appear to show preferential binding of nanoparticles to tail-spike domains, so the blocking of host receptor-binding domains as the sole mechanism for loss of infectivity seems unlikely. It is conceivable that the binding effect places nanoparticles in close proximity to phage, or host receptor proteins during infection, so that Ag^+, being shed continuously from the nanoparticles, produces a more focused, localized deleterious effect on phage attachment. Ag^+ is known to complex with the sulfur groups of certain amino acids (i.e. methionine and cysteine) and in ways that can interfere with structure and function of proteins (Behra et al., 2013**).** Differences in the number of methionine and cysteine residues in tail-spike domains, tail needle proteins, or host secondary receptor proteins, may also account for the differences in Ag^+ sensitivity observed between RG2014, P22, 9NA, SP6 and SF6. The mutant phages also appear to display higher levels of aggregation in TEM when nanoparticles, and the ability to bind them, are present. They, in fact, appear stuck together by a single nanoparticle linkage in the majority of images. This may also reduce infectivity, although in direct titers (as opposed to phages used in growth curves), phages incubated with nanoparticles for 30 min did not show difference in PFU. If co-aggregation of nanoparticles and phage were the issue, one would expect to see loss in titer there as well.

3.7. Effect of Ag^+ on phage infectivity

To assess the extent to which free silver ions released from nanoparticles affect phage infectivity, nanoparticles were removed from silver nanoparticle solutions that had been mixed in DI water or SMG buffer, by centrifugation. These supernatants were analyzed for the presence of silver ions using ICP-MS analysis and the results are shown in Table 2. It is notable that when nanoparticle solutions are diluted 2X into SMG buffer for 30 min, the Ag^+ concentration is substantially lower (72% lower) than when diluted into H_2O. Ag^+ and can form complexes with the Cl^- and $SO^{2-}4$ in SMG buffer to form insoluble products (e.g. AgCl and Ag_2S) **(**Behra et al., 2013**)** This would explain the resulting drop in [Ag^+] since these products would conceivably be pelleted out of solution with the nanoparticles upon centrifugation.

The solution obtained from centrifugation of bare nanoparticles in 0.5X SMG, containing 0.26 mg/L Ag^+ and small soluble products but no nanoparticles, was used to incubate phages RG2014, P22, and 9NA to a final Ag^+ concentration of 0.005 mg/L for inclusion in one-step growth curve experiments. Exposure to Ag^+ under these conditions reduced the PFU of RG2014 by 43% ± 7.5 [n = 3] ($p < 0.05$), 9NA by 24% ± 4 [n = 3] ($p < 0.05$), and P22 by 27% ± 2 [n = 3] ($p < 0.05$) (Figs. 4b−3.)**.** These results suggest the presence of silver ions (Ag^+) has a significant effect on infection of the phages tested, regardless of any silver ion chelating/reactive properties present in the growth media or phage/NP incubation buffers. The Ag^+ inhibition of P22 and 9NA, which are not observed to bind to

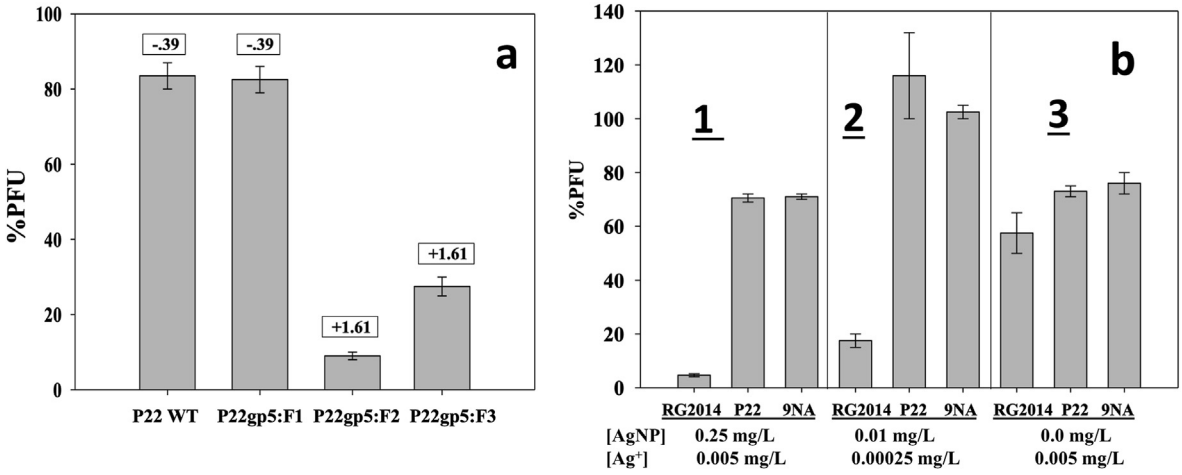

Fig. 4. (a) [n = 3] Post growth curve %PFU of mutant phages exposed to Bare AgNPs in 1X TM buffer. Boxed values represent the charge number of the last 10 amino acids of the coat protein at pH = 7.5 (Q of C-terminus). (b) [n = 3] Post growth curve %PFUs of infection with phages (in .5X SMG) exposed to: 1.) Conditions identical to the other bare AgNP/phage interaction growth curve experiments. 2.) a bare AgNP concentration that is diluted 25X after incubation with phage, and 3.) an identical volume of centrifuged bare AgNP supernatant used to incubate with phage. Concentration values given are those present in the infected 1 mL culture before the wash step. Error bars indicate standard deviation.

Table 2
Ag^{2+} concentrations in the supernatant.

Coating	Buffer	[Ag^{2+}] ppm	RSD
Bare	2 mM Na-citrate	0.93	3.6
PVP	H_2O	1.83	3.5
Bare	1 mM Na-Citrate, 0.5X SMG*	0.26	2.2
PVP	H_2O, 5X SMG*	0.21	2.8

10mn AgNP particle solutions, cleared by centrifugation of NPs, and Ag^+ quantified by ICP-MS.
RSD is the Relative Standard Deviation *0.5 SMG is (25 mM Tris pH7.5, 5 mM $MgSO_4$, 50 mM NaCl).

nanoparticles, is similar in degree to that when exposed to non-centrifuged nanoparticle solution. RG2014 show inhibitory effects from Ag^+ as a 43% ± 7.5 loss of PFU after 70 min of infection, but up to 96% ± 4.5 [n = 3] ($p < 0.05$ [(Figs. 4b–1) when incubated with nanoparticle solutions (not centrifuged). Since nanoparticles bind to RG2014, this further suggests that the greater inhibitory effects may be due to the increased proximity of nanoparticles to the phage and/or the host during infection, and thus greater localized exposure to Ag^+.

The inhibitory effects from Ag^+ seem to be in part due to action on host, rather than viral, proteins. In another experiment, a phage concentration 25X of that used in the other growth curve experiments was incubated with 10 mg/L nanoparticles, after which they were used to infect host stains at the typical MOI of 0.0625 (Fig. 4b). This dilutes the amount of nanoparticle solution in the 1 mL culture 25X, where effects from Ag^+ and nanoparticles are predicted to be negligible (Behra et al., 2013). RG2014 goes onto produce an 85% ± 3 [n = 3] ($p < 0.05$) reduction in PFU, whereas P22 and 9NA infected with normal efficiency [n = 3] ($p > 0.05$). This provides further evidence that the nanoparticles are bound to RG2014, since a similar degree of inhibitory effect is produced before, or after, dilution. Also, since P22 and 9NA, which do not bind to nanoparticles, did not produce the smaller ~30% inhibition of infection from Ag^+ as previously observed when the nanoparticle solution is not diluted (Fig. 4b), this implies the effects are a result of Ag^+ interacting with host.

4. Conclusions

Bacteriophages are highly diverse with unique properties and means of infection and are affected by nanoparticles in different ways. This report doesn't seek to explore the interactions between every combination of AgNPs and phages, or describe the mechanism for every possible effect. Rather, it describes limited examples of interactions to lay the groundwork for future research. It provides 1.) the first experimental evidence of effects from silver AgNPs on lytic growth curves of selected phages, (2) experimental evidence that some phages are affected and others are not by metal AgNPs and, (3) a small degree of mechanistic understandings of some components of inhibition using comparative genetics and targeted DNA editing. The experimentally observed interactions between nanoparticles, PVP, and bacteriophage virions reveal effects on infection efficiency which confer a clear fitness disadvantage (or advantage in the case of nanoparticles coated with PVP) to certain types of phages with the potential to affect microbial diversity. In these experiments, AgNPs and their ions are also shown to significantly affect phages at concentrations and incubation times in culture low enough to not affect growth of their host, as inferred by the AgNP bacteriocidal controls used in this study. The ability to predict which species of phage is sensitive to nanoparticles and/or their ions based off of simple coat protein sequence and structural predictions may answer questions regarding the populations affected. Further insights into the types and concentrations of nanoparticles required to manifest these effects will answer questions regarding the degree of impact as well.

Declaration of competing interest

The authors declare that they have no known competing financial interests or personal relationships that could have appeared to influence the work reported in this paper.

Acknowledgments

This study was supported by U.S National Science Foundation Grant 1600598. Views and opinions expressed or discussed in this manuscript are solely those of the authors and do not necessarily represent the funding agency. We highly appreciate Dr. Casjens Sherwood's (Department of Pathology, University of Utah) help for his useful pre-submission review and comments.

Appendix A. Supplementary data

Supplementary data to this article can be found online at https://doi.org/10.1016/j.watres.2020.115900.

References

Argov, T., Azulay, G., Pasechnek, A., Stadnyuk, O., Sapir, S., Borovok, I., Sigal, N., Herskovits, A., 2017. Temperate bacteriophagess as regulators of host behavior. Curr. Opin. Microbiol. 38, 81–87.

Ashelford, K., Norris, S., Fry, J., Bailey, M., Day, M., 2000. Seasonal population dynamics and interactions of competing bacteriophagess and their host in the rhizosphere. Appl. Environ. Microbiol. 66 (10), 4193–4199.

Baker, T., Tyler, C., Galloway, T., 2014. Impacts of metal and metal oxide nanoparticles on marine organisms. Environ. Pollut. 186, 257–271.

Beddow, J., Stolpe, B., Cole, P., Lead, J., Sapp, M., Lyons, B., Colbeck, I., Whitby, C., 2014. Effects of engineered silver nanoparticles on the growth and activity of ecologically important microbes. Environ. Microbiol. Rep. Oct 6 (5), 448–458.

Behra, R., Sigg, L., Clift, M., Herzog, F., Minghetti, M., Johnston, B., Petri-Fink, A., Rutishauser, B., 2013. Bioavailability of silver nanoparticles and ions: from a chemical and biochemical perspective. J. R. Soc. Interface (87), 10. Oct 6.

Benn, T., Westerhoff, P., 2008. Nanoparticle silver released into water from commercially available sock fabrics. Environ. Sci. Technol. 42, 4133–4139.

Bhattacharjee, S., 2016. DLS and zeta potential - what they are and what they are not? J. Contr. Release 235, 337–351. Aug 10.

Bhattacharjee, A., Choi, J., Motlagh, A., Mukherji, S.T., Goel, R., 2015. Bacteriophage therapy for membrane biofouling in membrane bioreactors and antibiotic-resistant bacterial biofilms. Biotechnol. Bioeng. 112 (8), 1644–1654.

Bhattacharjee, A., Motlagh, A., Gilcrease, E., Islam, M., Casjens, S., Goel, R., 2017. Complete genome sequence of lytic bacteriophages RG-2014 that infects the multidrug resistant bacterium Delftia tsuruhatensis ARB-1. Standards in Genomic Sci. 12 (1), 82.

Breitbart, M., 2012. Marine viruses: truth or dare. Ann. Rev. Marine Sci. 4, 425–448.

Brussaard, C., Wilhelm, S., Thingstad, F., Weinbauer, M., Bratbak, G., Heldal, M., Kimmance, S., Middelboe, M., Nagasaki, K., Paul, J., 2008. Global-scale processes with a nanoscale drive: the role of marine viruses. ISME J. 2, 575–578.

Casjens, S., Winn-Stapley, D.A., Gilcrease, E.B., Morona, R., Kühlewein, C., Chua, J.E., Manning, P.A., Inwood, W., Clark, A.J., 2004. The chromosome of Shigella flexneri bacteriophages Sf6: complete nucleotide sequence, genetic mosaicism, and DNA packaging. J. Mol. Biol. 339 (2), 379–394. May 28.

Casjens, S., Jacobs-Sera, D., Htfull, G., Hendrix, R., 2015. Genome sequence of *salmonella enterica* phages Det7. Genome Announc. May-Jun 3 (3) e00279-15.

Casjens, S., Leavitt, J., Hatfull, G., Hendrix, R., 2014. Genome sequence of *salmonella* phages 9NA. Genome Announc. Jul-Aug 2 (4) e00531-14.

Corbisier, P., van der Lelie, D., Borremans, B., Provoost, A., de Lorenzo, V., Brown, N.L., et al., 1999. Whole cell-and protein-based biosensors for the detection of bioavailable heavy metals in environmental samples. Anal. Chim. Acta 387 (3), 235–244.

Dakal, T., Kumar, A., Majumdar, R., Yadav, V., 2016. Mechanistic basis of antimicrobial 689 actions of silver nanoparticles. Front. Microbiol. 16 November 2016.

Das, D., Chakraborty, A., Bhattacharjee, S., Dey, S., 2013. Biosynthesis of stabilized gold nanoparticle using an aglycone flavonoid, quercetin. J. Exp. Nanosci. 8 (4), 649–655.

Dobbins, A., George, M., Basham, D., Ford, M., Houtz, J., Pedulla, M., Lawrence, J., Hatfull, G., Hendrix, R., 2004. Complete genomic sequence of the virulent *salmonella* bacteriophages SP6. J. Bacteriol. Apr 186 (7), 1933–1944.

Duda, R., Martincic, K., Hendrix, R., 1995. Genetic basis of bacteriophages HK97 prohead assembly. J. Mol. Biol. 247 (4), 636–647, 7 April.

Dukhovich, F.S., Darkhovskii, M.B., Gorbatova, E.N., Kurochkin, V.K., 2003. Molecular Recognition: Pharmacological Aspects. Nova Science Publishers, New York, NY.

Earnshaw, W., Casjens, S., Harrison, S., 1976. Assembly of the head of bacteriophages P22: x-ray diffraction from heads, proheads and related structures. J. Mol. Biol. 104, 387–410.

Gombotz, W., Pankey, S., Phan, D., Drager, R., Donaldson, K., Antonsen, K., Hoffman, A., Raff, H., 1994. The Stabilization of a Human IgM Monoclonal Antibody with Poly(vinylpyrrolidone) May, 11, pp. 624–632, 5.

Hockett, K.L., Baltrus, D.A., 2017. Use of the soft-agar overlay technique to screen for bacterially produced inhibitory compounds. JoVE (119), e55064.

Hryc, C.F., Chen, D.H., Afonine, P.V., Jakana, J., Wang, Z., Haase-Pettingell, C., Jiang, W., Adams, P.D., King, J.A., Schmid, M.F., Chiu, W., 2017. Accurate model annotation of a near-atomic resolution cryo-EM map. Proc. Natl. Acad. Sci. U.S.A. 114, 3103–3108.

Huan-Xiang, Zhou, 2013. Polymer crowders and protein crowders act similarly on protein folding stability. FEBS (Fed. Eur. Biochem. Soc.) Lett. 587 (5), 394–397, 2013 Mar 1.

Juganson, K., Ivansk, A., Blinova, I., Mortimer, M., Kahru, A., 2015. NanoE-Tox: new and in-depth database concerning ecotoxicity of nanomaterials. Beilstein J. Nanotechnol. 6, 1788–1804.

Kapoor, S., Lawless, D., Kennepohl, P., Meisel, D., Serpone, N., 1994. Reduction and aggregation of silver ions in aqueous gelatin solutions. Langmuir 10 (9), 3018–3022.

Kenzaka, T., Tani, K., Sakotani, A., Tamaguchi, N., Nasu, M., 2007. High-frequency phages-mediated gene transfer among *Escherichia coli* cells, determined at the single-cell level. Appl. Environ. Microbiol. 73 (10), 3291–3299.

Kizziah, J.L., Manning, K.A., Dearborn, A.D., Wall, E.A., Klenow, L., Hill, R.L.L., Spilman, M.S., Stagg, S.M., Christie, G.E., Dokland, T., 2017. Cleavage and structural transitions during maturation of *staphylococcus aureus* bacteriophages 80 alpha and SaPI1 capsids. Viruses. Dec 9 (12), 384.

Kotay, S.M., Datta, T., Choi, J., Goel, R., 2011. Biocontrol of biomass bulking caused by Haliscomenobacter hydrossis using a newly isolated lytic bacteriophage. Water Res. 45, 694–704.

Krystiak-Baltyn, K., Martin, G., Stickland, A., Scales, P., Gras, S., 2017. Simulation of phages dynamics in multi-reactor models of complex wastewater treatment systems. Biochem. Eng. J. 122, 91–102.

Levard, C., Mitra, S., Yang, T., Jew, A., Badireddy, A., Lowry, G., Brown, G., 2013. Effect of chloride on the dissolution rate of silver nanoparticles and toxicity to E. coli. Environ. Sci.Technol. 47 (11), 5738–5745.

Liu, Y., Hardie, J., Zhang, X., Rotello, V., 2017. Effects of engineered nanoparticles on the innate immune system. Semin. Immunol. 34, 25–32. Dec.

Marinelli, L., Hatfull, G., Piuri, M., 2012. Recombineering. A powerful tool for modification of bacteriophage genomes Bacteriophage 2 (1), 5–14. Jan 1.

Massarsky, A., Dupuid, L., Taylor, J., Eisa-Beygi, S., Strek, L., Trudeau, V., Moon, T., 2013. Assessment of nanosilver toxicity during zebrafish (*Danio rerio*) development. Chemosphere 92, 59–66.

Mathieu, J., Yu, P., Zuo, P., Da Silva, M.L., Alvarez, P.J., 2019. Going viral: emerging opportunities for phage-based bacterial control in water treatment and reuse. Accounts Chem. Res. 52 (4), 849–857.

Matteson, A., Loar, S., Bourbonniere, R., Wilhelm, S., 2011. Molecular enumeration of an ecologically important cyanophages in a laurentian great lake. Appl. Environ. Microbiol. 77 (19), 6772–6779.

McClelland, M., Sanderson, K., Spieth, J., Clifton, S., Latreille, P., Courtney, L., Porwollik, S., Ali, J., Dante, M., Du, F., Hou, S., Layman, D., Leonard, S., Nguyen, C., Scott, K., Holmes, A., Grewal, N., Mulvaney, E., Ryan, E., Sun, H., Florea, L., Miller, W., Stoneking, T., Nhan, M., Waterston, R., Wilson, R., 2001. Complete genome sequence of *Salmonella enterica serovar Typhimurium* LT2. Nature 413, 852–856.

Miller, J.H., 1972. Experiments in molecular genetics. Cold Spring Harbor Laboratory. Cold Spring.

Mirzaei, A., Janghorban, K., Hashemi, B., Bonyani, M., Leonardi, S., Neri, G., 2017. Characterization and optical studies of PVP-capped silver nanoparticles. J. Nanostruct. Chem. 7 (1), 37–46.

Nielsen, P., Kragelund, C., Seviour, R., Nielsen, J., 2009. Identity and ecophysiology of filamentous bacteria in activated sludge. FEMS Microbiol. Rev. 33, 969–998.

O'Callaghan, D., Charbit, A., 1990. High Efficiency Transformation of Salmonella typhimurium and Salmonella typhi by Electroporation August, 223, pp. 156–158, 1.

Oberdorster, G., Stone, V., Donaldson, K., 2007. Toxicology of nanoparticles: a historical perspective. Nanotoxicology 1, 2–25.

Pedulla, M., Ford, M., Karthikeyan, T., Houtz, J., Hendrix, R., Hatfull, G., Poteete, A., Gilcrease, E., Winn-Stapley, D., Casjens, S., 2003. C°rrected sequence of the bacteriophages P22 Genome. J. Bacteriol. Feb 185 (4), 1475–1477.

Seil, J., Webster, T., 2012. Antimicrobial applications of nanotechnology: methods and literature. Int. J. Nanomed. 7, 2767–2781.

Servid, A., Jordan, P., O'Neil, A., Prevelige, P., Douglas, T., 2013. Location of the bacteriophages P22 coat protein C-terminus provides opportunities for the design of capsid-based materials. Biomacromolecules (9), 14, 3 Sep. 9.

Shafiai, F., Thompson, T., 1964. Calcium requirement for proliferation of bacteriophages Journal of Bacteriology 88 (2), 293–296. August, 1964.

Sheng, Z., Liu, Y., 2017. Potential impacts of silver nanoparticles on bacteria in the aquatic environment. J. Environ. Manag. 191, 290–296.

Skoglund, S., Hedberg, J., Yunda, E., Godymchuk, A., 2017. Difficulties and flaws in performing accurate determinations of zeta potentials of metal nanoparticles in complex solutions—four case studies. PLoS One journals.plos.org.

Suttle, A., 2005. Viruses in the sea. Nature 437, 356–361.

Suttle, A., 2007. Marine viruses — major players in the global ecosystem. Nat. Rev. Microbiol. 5, 801–812.

Swanson, M., Fraser, G., Daniell, T., Torrance, L., Gergory, P., Taliansky, M., 2009. Viruses in soils: morphological diversity and abundance in the rhizosphere. Ann. Appl. Biol. 155, 468–477.

Tang, L., Gilcrease, E., Casjens, S., Johnson, J., 2006. Highly discriminatory binding of capsid-cementing proteins in bacteriophage. L Structure 14, 837–845.

Tokuno, S.I., Gough, M., 1975. Host influence on the activity of genes c1 and c3 in regulating the decision between lysis and lysogency in bacteriophage P22. J. Virol. Nov 16 (5), 1184–1190.

Tresset, G., Chen, J., Chevreuil, M., Nhiri, N., Jacquet, E., Lansac, Y., 2017. Two-dimensional phase transition of viral capsid gives insights into subunit interactions. Phys. Rev. Appl. 7, 014005.

Vazquez-Munoz, R., Berrego, B., Juarez-Moreno, K., Garcia-Garcia, M., Morales, J., Bogdanchikova, N., Huerta-Saquero, A., 2017. Toxicity of silver nanoparticles in biological systems: does the complexity of biological systems matter? Toxicol. Lett. 276, 11–20.

Wang, X., Kim, Y., Hong, S., Pokusaeva, K., Sturino, J., Wood, T., 2010. Cryptic prophagess help bacteria cope with adverse environments. Nat. Commun. 1, 147.

Weinbauer, M., Rassoulzadegan, F., 2004. Are viruses driving microbial diversification and diversity? Environ. Microbiol. 6, 1–11.

Wittebole, X., De Roock, S., Opal, S., 2014. A historical overview of bacteriophages therapy as an alternative to antibiotics for the treatment of bacterial pathogens. Virulence 5 (1), 226–235.

Wong, B., Hu, Q., Baeg, G., 2017. Epigenetic modulations in nanoparticle-mediated toxicity. Food Chem. Toxicity 109, 746–752.
Xing, R., Li, K., Zhou, Y., Su, Y., Yan, S., et al., 2016. Impact of fluorescent silicon nanoparticles on circulating hemolymph and hematopoiesis in an invertebrate model organism. Chemosphere 159, 628–637.
Yang, Y., Li, M., Michels, C., Moreira-Soares, H., Alvarez, P.J., 2014. Differential sensitivity of nitrifying bacteria to silver nanoparticles in activated sludge. Environ. Toxicol. Chem. Oct 33 (10), 2234–2239.
Yong, D., et al., 2009. Characterization of a new metallo-β-lactamase gene, bla_{NDM-1}, and a novel erythromycin esterase gene carried on a unique genetic structure in *Klebsiella pneumoniae* sequence type 14 from India. Antimicrob. Agents Chemother. 53, 5046–5054.
Zhang, C., Hu, Z., Li, P., Gajaraj, S., 2016. Governing factors affecting the impacts of silver nanoparticles on wastewater treatment. Sci. Total Environ. 572, 852–873.